Journal of Applied Physics ARTICLE pubs.aip.org/aip/jap

Overcoming the doping limit in GaAs by ion implantation and pulsed laser melting

Cite as: J. Appl. Phys. **135**, 045703 (2024); doi: 10.1063/5.0190600
Submitted: 7 December 2023 · Accepted: 4 January 2024 ·
Published Online: 26 January 2024

Kin Man Yu,[1,2,a)] M. A. Scarpulla,[3] Chun Yuen Ho,[4] O. D. Dubon,[2,5] and W. Walukiewicz[2,b)]

AFFILIATIONS

[1]Department of Physics, City University of Hong Kong, Kowloon, Hong Kong
[2]Materials Sciences Division, Lawrence Berkeley National Laboratory, Berkeley, California 94720, USA
[3]Department of Materials Science and Engineering, The University of Utah, Salt Lake City, Utah 84112, USA
[4]Centre for Advanced Photovoltaics and Thin-Film Energy Devices, Mads Clausen Institute, University of Southern Denmark, DK-6400 Sønderborg, Denmark
[5]Department of Materials Sciences and Engineering, University of California, Berkeley, California 94720, USA

Note: This paper is part of the special topic, Defects in Semiconductors 2024.
[a)]**Author to whom correspondence should be addressed:** kinmanyu@cityu.edu.hk
[b)]**Deceased.**

ABSTRACT

Most semiconductors exhibit a saturation of free carriers when heavily doped with extrinsic dopants. This carrier saturation or "doping limit" is known to be related to the formation of native compensating defects, which, in turn, depends on the energy positions of their conduction band minimum and valence band maximum. Here, we carried out a systematic study on the *n*-type doping limit of GaAs via ion implantation and showed that this doping limitation can be alleviated by the transient process of pulsed laser melting (PLM). For *n*-type doping, both group VI (S) and amphoteric group IV (Si and Ge) dopants were implanted in GaAs. For comparison, p-type doping was also studied using Zn as the acceptor. Implanted dopants were activated by the PLM method, and the results are compared to rapid thermal annealing (RTA). Our results reveal that for all n-type dopants, while implantation followed by the RTA results in a similar saturation electron concentration of $2–3 \times 10^{18}$ cm^{-3}, the transient PLM process is capable of trapping high concentration of dopants in the substitutional site, giving rise to a carrier concentration of $>10^{19}$ cm^{-3}, exceeding the doping limit of GaAs. However, due to scatterings from point defects generated during PLM, the mobility of n-type GaAs after PLM is low (~80–260 cm^2/V s). Subsequent RTA after PLM (PLM + RTA) is able to remove these point defects and recover the mobility to ~1000–2000 cm^2/V s. The carrier concentrations of these PLM + RTA samples are reduced but are still a factor of 3 higher than RTA only GaAs. This can be understood as the dopants are already incorporated in the substitutional site after PLM; they are less likely to be "deactivated" by subsequent RTA. This work is significant to the understanding of doping mechanisms in semiconductors and provides a means for device applications, which require materials with ultra-high doping.

INTRODUCTION

Functionalities of semiconductors depend critically on their controllable conductivity through doping. However, the "dopability" of some semiconductors is severely limited as their free carrier concentration exhibits a saturation when the dopant concentration is high. This doping limitation is related to the positions of their conduction minimum (CBM) and valence band maximum (VBM), which affect the formation energies of native defects.[1–7] Consequently, the fundamental mechanisms that lead to the practical doping limits in semiconductors continue to be a subject of current interest. In general, the "doping limit" refers to a maximum carrier concentration, which corresponds to a maximum Fermi level position ($E_{F,max}$). When the doping exceeds this concentration, simultaneous the formation of compensating native defects occurs, which limits the carrier concentration.[7] Walukiewicz developed a phenomenological model, the amphoteric native defect model (ADM), which relates formation energies of donor and acceptor native

defects to the location of the Fermi level E_F with respect to the Fermi level stabilization energy E_{FS}.[8] E_{FS} is E_F at which the formation energies of native donor and acceptor defects are equal and was found to be constant for all semiconductors located at ~4.9 eV below the vacuum level (E_{vac}). When a semiconductor is doped with increasing dopant concentration, the electron (hole) concentration increases so that the E_F moves above (below) E_{FS}. As a result, the formation energy of compensating native acceptor (donor) defects decreases and eventually becomes energetically more favorable, hence limiting the doping efficiency. Consequently, the electron (hole) concentration saturates toward a maximum electron (hole) concentration. The ADM has been shown to provide qualitative predictions of the maximum free electron (hole) concentration n_{max} (p_{max}) achievable by doping, corresponding to $E_{F,max}$ at ~1 eV above (below) E_{FS} in a wide variety of III–V[9,10] and II–VI[9,11–14] semiconductors. In essence, this suggests that semiconductors with the CBM (VBM) located close to E_{FS} can be easily doped *n*-type (*p*-type). For most wide gap metal oxides, such as ZnO, CdO, and In_2O_3, their CBM is $\lesssim$0.5 eV above, while the VBM is >2.5 eV below E_{FS}, which makes them easily doped *n*-type to a high electron concentration (>10^{20} cm^{-3}), but their p-type doping is very difficult, if not impossible.[9,14,15]

The position of the CBM and VBM of GaAs with reference to E_{vac} is ~ -4.07 eV ($\sim E_{FS} + 0.83$ eV) and -5.5 eV ($E_{FS} - 0.6$ eV), respectively. In other words, $E_{F,max}$ for *n* (*p*-)-type GaAs is at ~0.17 eV above (~0.4 eV below) the CBM (VBM). Thus, according to the ADM, GaAs can be doped heavily *p*-type (>10^{20} cm^{-3}) but its *n*-type doping is limited (<10^{19} cm^{-3}). It has been shown that in *n*-type GaAs, the electron concentration saturates at the range of ~10^{18}–10^{19} cm^{-3}. This corresponds to E_F located at <0.2 eV above the CBM or at ~ < 1.1 eV above E_{FS},[16] in good agreement with the ADM. Such a limitation in doping can to some extent be overcome through utilizing some nonequilibrium epitaxial growth methods, manipulating the growth environment, as well as the doping techniques such as co-doping[17–19] and implantation followed by rapid annealing processes.[20–22] In particular, n_{max} values in GaAs up to 2×10^{19} cm^{-3} were demonstrated using transient annealing processes such as pulse electron beam annealing.[23] This high n_{max} value exceeds the "doping limit" of *n*-type GaAs with E_F at ~E_{FS} + 1.2 eV.

Pulsed laser annealing (PLA) is another transient annealing process, which has been studied extensively in the late 1970s and early 1980s for the dopant activation and damage recovery of ion implanted Si and GaAs.[22,24–28] Typically, a short (μs to ns), intense laser pulse incidents on the surface of the sample and the semiconductor absorbs the energy and locally heats the material to a high temperature. In the case when the energy fluence is high enough to locally melt the material, a rapid melt and recrystallization of the semiconductor occurs, which is more commonly referred to as pulsed laser melting (PLM). For implanted semiconductors, the melting of the implant-damaged or amorphized layer is induced by the near surface absorption of intense (pulsed) laser radiation, and the melted layer rapidly regrows epitaxially from the liquid. In the PLM of implanted samples, the melted layer depth must exceed the damaged depth so that high quality liquid phase epitaxy (LPE) can occur at the solid–liquid interface from the perfect crystalline bulk. Since the LPE process occurs on a much shorter time scale, typically between 10^{-8}–10^{-6} s, impurities do not have sufficient time to diffuse and segregate, and, hence, the density of impurities way above the solubility limit can be incorporated in the lattice (solute trapping). For example, Mn and N with concentration up to several mol. % can be incorporated in GaAs via ion implantation and PLM, forming, respectively, ferromagnetic semiconductor and dilute GaAs nitride layers.[29–31] It was also shown that using the PLM method, amorphous layers of GaAs formed by high dose implantation could be regrown into single crystals with electrical activities of dopants well above those achievable by furnace annealing.[25,26,27] We also note that the doping of Si by ion implantation followed by PLM was widely studied from the 1970s through the 1990s, and readers were referred to a recent review by Lim and Williams [28] and references therein. However, due to the small bandgap of Si and that E_{FS} is only slightly closer to the VBM, heavy doping with both *n* and *p* of >10^{20} cm^{-3} was achievable with both rapid thermal annealing (RTA) and furnace annealing in Si. Hence, improvements in the carrier concentration using PLM in Si were not dramatic.

In this work, we report on a comprehensive investigation on the *n*- and *p*-type doping of GaAs by ion implantation and PLM. We find that the PLM process is effective in incorporating dopants in the proper sites, which leads to an *n*-type doping exceeding the "doping limit" in GaAs. However, as previously shown in the formation of dilute GaNAs highly mismatched alloys by N implantation and PLM,[30,31] a high density of residual defects was present after PLM, which resulted in a low mobility in these samples. While post-PLM rapid thermal annealing (PLM + RTA) is effective in restoring the carrier mobility by removing these defects, it also reduces the carrier concentration. When compared to the RTA only samples, the carrier concentration of the PLM + RTA samples is still significantly higher, which can be attributed to the "solute trapping" of the PLM process, which makes the removal of these dopants from the substitutional site more difficult during RTA. In direct contrast, effects of PLM on the *p*-type doping by Zn implantation are much less significant, which can be attributed to the close proximity of the VBM with the E_{FS} in GaAs, making *p*-type doping more effective and the formation of compensating donors less likely.

EXPERIMENT

Both donor (S, Si, and Ge) and acceptor (Zn) species were implanted in semi-insulating GaAs wafers. The implantation conditions, including energy, total dose, and approximate profiles of various dopant species, are tabulated in Table I. Except for the S doping, multi-energy implantation was carried out to produce a relatively flat dopant distribution (box shape) over a depth of ~0.08–0.24 μm. Dopant profiles with peak atomic concentrations ranging from 1.6×10^{19} to 6×10^{20} cm^{-3} were studied. All implantations were carried out at room temperature using a beam current of ~0.2–0.5 $\mu A/cm^2$. Calculated atomic profiles of the implanted samples are shown in Fig. 1.

After implantation, pulsed laser melting (PLM) was carried out in air using an XeCl excimer laser ($\lambda = 308$ nm) with a pulse duration of ~30 ns. The pulsed laser beam was homogenized through a multi-prism homogenizer with a fluence at the sample

TABLE I. Implantation conditions (energy, dose, and approximate profiles) of various dopant species in GaAs studied in this work.

Dopants	Total dose (cm^{-2})	Energy (keV)	Dopant concentration
S	1.0×10^{15} (lo) 5.0×10^{15} (hi)	60 60	~0.08 μm with ~1.2×10^{20} cm^{-3} ~0.08 μm with ~6.0×10^{20} cm^{-3}
Si	1.53×10^{15}	175 keV 1.1×10^{15} + 78 keV 3.1×10^{14} + 35 keV 1.25×10^{14}	~0.24 μm with ~6.4×10^{19}/cm^3
Ge	8.1×10^{15}	340 keV 6.4×10^{15} + 100 keV 1.7×10^{15}	~0.22 μm with ~3.7×10^{20}/cm^3
Zn	4.36×10^{15}	140 keV 3.6×10^{15} + 45 keV 7.6×10^{14}	~0.08 μm with ~4.7×10^{20}/cm^3

ranging from 0.35 to 0.45 J/cm^2. The laser fluence used was determined from previous work[31] so that the melt depth can exceed the implant-damage region, to ensure regrowth from the bulk GaAs lattice. The melt duration (τ_{melt}) was determined by monitoring the time resolved reflectivity (TRR) of the samples using an argon-ion laser. In order to investigate the stability of the electrical properties, after PLM, some of the samples were further annealed by rapid thermal annealing (RTA) at temperatures T_{RTA} between 600 and 950 °C for a duration of 10–60 s in flowing N_2.

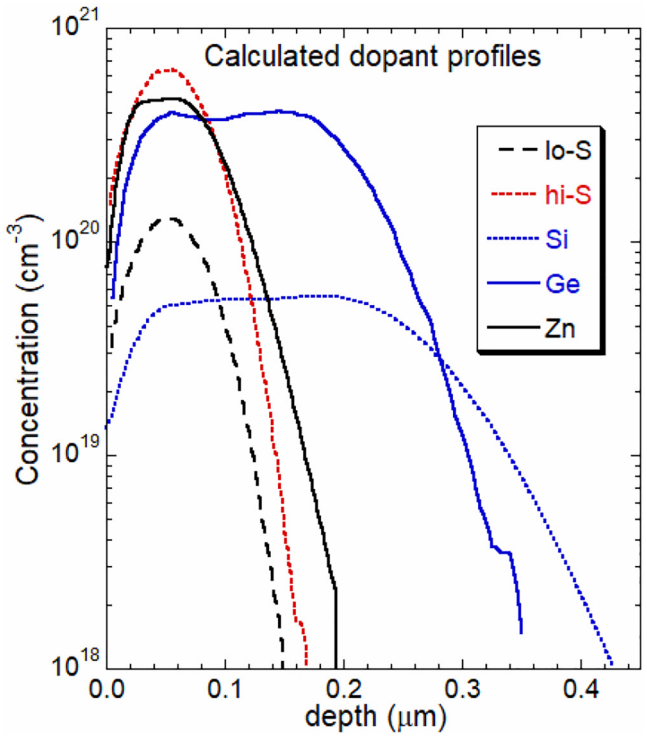

FIG. 1. Calculated atomic distribution profiles of several dopants implanted in GaAs.

The ion implantation damage and recovery of the samples were studied by channeling Rutherford backscattering spectrometry (c-RBS) in the ⟨100⟩ direction using a 2 MeV He^+ beam at a backscattering angle of 165°. The electrical properties of the samples were measured by the Hall effect in the *van der Pauw* configuration with a 0.55 T magnetic field at room temperature. The bulk carrier concentration was estimated by assuming a uniform distribution over the calculated implantation range. Since the PLM was carried out in air, it is possible that As loss during PLM may modify the GaAs surface, which may, in turn, complicate the Hall measurement results. However, no noticeable anomalies in the electron concentration and mobility of GaAs surfaces after PLM in air were observed in previous reports using differential Hall measurements.[32,33] Electrochemical capacitance–voltage (ECV) measurements were also carried out for some samples using a BioRad PN4300 Semiconductor Profile Plotter to obtain net space charge concentration profiles. In ECV profiling, an electrolyte was used as a Schottky contact to the semiconductor surface. Depth profiling was made possible by controllably removing the material by electrochemical etching.[34] In this work, a 0.2 M NaOH: EDTA solution was used as the electrolyte.

RESULTS AND DISCUSSION

Figure 2(a) shows the c-RBS spectra of 60 keV S implanted GaAs samples with total doses of 1×10^{15} (lo) and 5×10^{15} cm^{-2} (hi) aligned along the ⟨100⟩ axial direction. The ⟨100⟩ aligned spectrum from an unimplanted sample is also shown for comparison. The ⟨100⟩ aligned backscattering yields from implanted samples are much higher than those of the unimplanted sample, which suggests that significant dechanneling of the ion beam from implantation damage occurs. These implant-induced defects increase with ion dose and are confined within the surface 100 nm layer. Since the ⟨100⟩ yields for both implanted samples do not reach the random level, the damaged surface layer is still crystalline with a high level of crystalline and point defects. Figure 2(b) compares the c-RBS spectra from the as-implanted hi-S sample with that after PLM with a laser fluence of 0.35 J/cm^2. Figure 2(b) shows that the c-RBS yields decrease dramatically after PLM with no noticeable damage peak at the sample surface. This suggests that

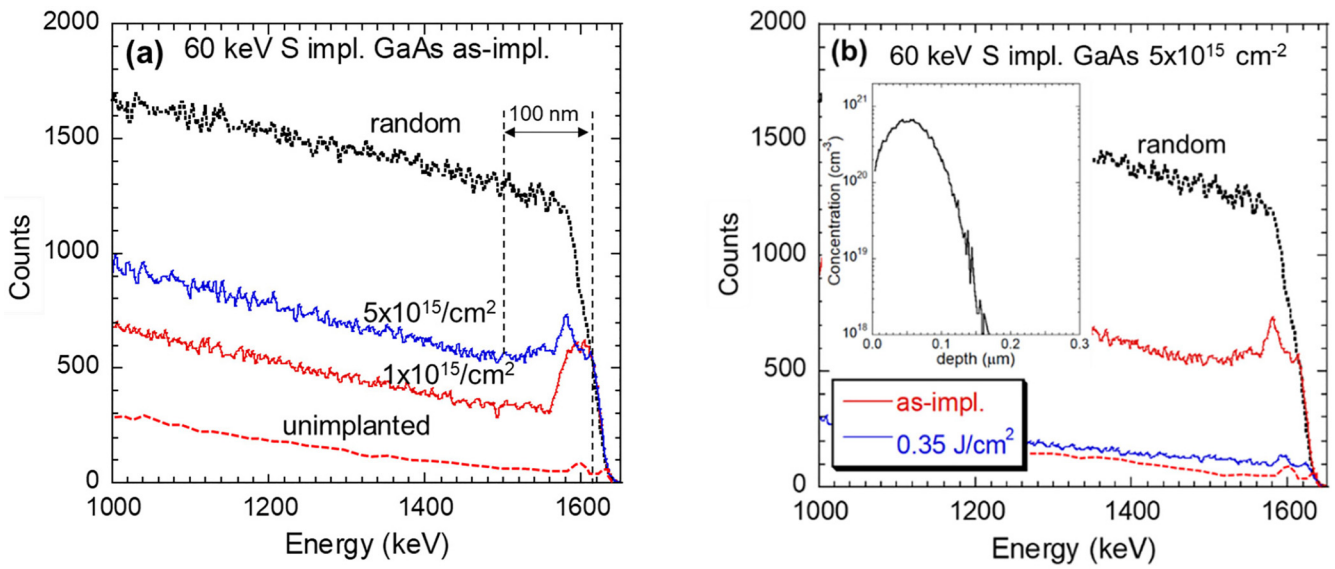

FIG. 2. (a) c-RBS spectra from 60 keV S implanted GaAs samples with total doses of 1×10^{15} and 5×10^{15} cm^{-2} aligned along the ⟨100⟩ axial direction. The ⟨100⟩ aligned spectrum from an unimplanted sample is also shown for comparison. (b) ⟨100⟩ c-RBS spectra from the 60 keV S implanted GaAs samples with a total dose of 5×10^{15} as-implanted and after PLM with a laser fluence of 0.35 J/cm^2. The inset in (b) shows the calculated S atomic distribution profile.

the PLM fluence is sufficient to melt the entire damaged region and the regrowth proceeds from the bulk GaAs to the surface. This is consistent with our previous work on the synthesis of highly mismatched dilute GaAs nitrides,[30,31] which demonstrated that a laser fluence >0.3 J/cm^2 is sufficient to melt GaAs up to ~150 nm. However, the c-RBS yields from the surface layer of the PLM sample are still slightly higher than those from unimplanted GaAs, which reveals that the regrown layer still has a high concentration of defects, most likely native defects such as vacancies and antisites. The presence of a high concentration of defects in these PLM samples would strongly affect their electrical properties.

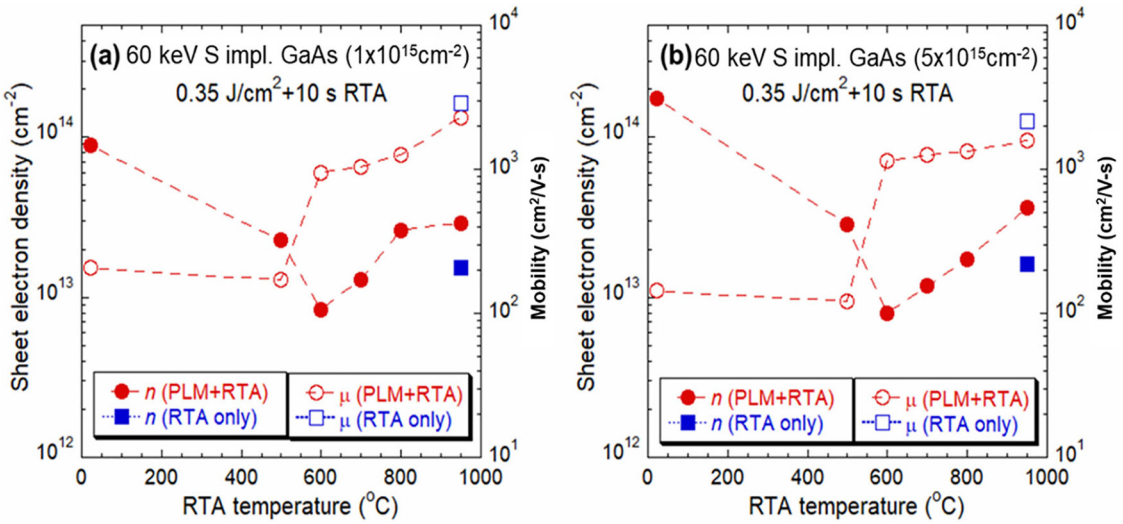

FIG. 3. Hall effect measurements showing the sheet electron density n_s and mobility μ of the (a) 1×10^{15} and (b) 5×10^{15} cm^{-2} s implanted GaAs samples after PLM followed by RTA (PLM + RTA) in the temperature range of 500–950 °C. The n_s and μ for samples after RTA at 950 °C for 10 s only are also shown for comparison.

The electrical properties of the lo- and hi-S implanted GaAs samples after PLM followed by RTA (PLM + RTA) in the T_{RTA} range of 500–950 °C were measured by the Hall effect, and the results are shown, respectively, in Figs. 3(a) and 3(b). The sheet electron density n_s and mobility μ for samples after RTA at 950 °C for 10 s only are also shown for comparison. We note that this is the typical RTA temperature needed to activate implanted dopants in GaAs. After RTA only, we see that both the lo- and hi-S samples have similar n_s of ~1.5–1.6 × 10^{13} cm^{-2}. This translates to low activation efficiency of ~1.5% and 0.3% of implanted S. The similar n_s despite the five times difference in the implanted S dose suggests that there is a saturation in the free electron concentration n_{sat} in these samples. Assuming a ~0.08 μm thick implanted layer, this corresponds to a $n_{sat} \sim 2 \times 10^{18}$ cm^{-3}. The Fermi level E_F can be related to the carrier concentration by the following expression:[11,35]

$$n = \frac{1}{3\pi^2}\int_{E_C/k_BT}^{\infty} \frac{\exp\,(z - E_F/k_BT)}{1 + \exp\,(z - E_F/k_BT)^2} k^3(z)dz, \quad (1)$$

where E_C is the energy of the CBM, k_B is the Boltzmann constant, $z = E_C/k_BT$, and k is the wavevector. Using Eq. (1), n_{sat} predicted by the ADM where $E_{F,max} \sim E_{FS} + 1$ eV (or at ~3.9 eV below E_{vac}) is ~5.6 × 10^{18} cm^{-3}. n_{sat} for the S implanted samples corresponds to E_F located at ~76 meV above the CBM. This is ~0.9 eV above E_{FS}, close to the electron saturation level but still below the $E_{F,max}$. The μ of the RTA only lo- and hi-S samples are 2900 and 2159 cm^2/V s, respectively, which are consistent with calculated and reported GaAs mobility at this electron concentration.[35] Note that the lower μ for the hi-S sample can be attributed to scatterings from compensating native defects or a higher level of residual implant-damage in the sample. These results suggest that compensating native acceptor defects are not entirely removed even after T_{RTA} at 950 °C.

After PLM, both samples have high n_s of 8.9 × 10^{13} and 1.75 × 10^{14} cm^{-2}, respectively, for the lo- and hi-S samples, corresponding to the activation efficiency of ~8.9% and 3.5%. The estimated electron concentration n is ~1 and 2.2 × 10^{19} cm^{-3}, exceeding the n_{sat} achieved after RTA only. The high n corresponds to $E_F \sim 0.4$ eV above the CBM or >1.2 eV above E_{FS}. However, the μ value of these PLM samples is relatively low, ~207 and 144 cm^2/V s, respectively, for the lo- and hi-S samples. These values are much lower than the μ of ~1000 cm^2/V s obtained for GaAs with comparable n.[35] This is, however, consistent with the c-RBS (Fig. 2), which shows that after PLM, the channeling yields are still significantly higher than those from unimplanted GaAs due to defects in the samples and likely arise from the laser melting-regrown process. These defects contribute to carrier scattering and reduce the carrier mobility. In order to remove these residual damages, RTA was carried out following PLM. Figure 3 shows that in general, similar behavior is observed as T_{RTA} increases after PLM; namely, n_s gradually decreases to a minimum value at ~600 °C and increases again at higher T_{RTA}, while μ shows a monotonic increase with T_{RTA}. The increase in μ with T_{RTA} is consistent with the reduction of defect scatterings due to the removal of defects at high temperature. The initial drop of n_s with increasing T_{RTA} up to 600 °C may be related to the reduction of native defects or complexes that also act as shallow donors (e.g., As vacancies V_{As}, Refs. 36 and 37) when the samples were annealed at

TABLE II. A summary of electrical properties of GaAs samples implanted with various donor species as tabulated in Table I followed by RTA, PLM, and PLM + RTA.

Dopants	Total dose (cm^{-2})	Annealing conditions		Sheet conc. n_s (×10^{13} cm^{-2})	Mobility μ (cm^2/V s)	Electron conc. n (×10^{18} cm^{-3})	E_F–E_c (eV)	Peak dopant conc. (×10^{18} cm^{-3})
S	1.0 × 10^{15} (lo)	RTA only	950 °C 10 s	1.53	2900	1.9	0.074	127
			950 °C 60 s	2.3	2324	2.9	0.098	
		PLM only	0.35 J/cm^2	8.93	207	11	0.26	
		PLM + RTA	950 °C 10 s	2.9	2300	3.6	0.115	
			950 °C 60 s	3.87	2005	4.84	0.143	
	5.0 × 10^{15} (hi)	RTA only	950 °C 10 s	1.6	2150	2.0	0.076	640
			950 °C 60 s	1.63	2830	2.0	0.076	
		PLM only	0.35 J/cm^2	17.4	144	22	0.40	
		PLM + RTA	950 °C 10 s	3.6	1600	4.5	0.135	
			950 °C 60 s	4.2	1940	5.25	0.151	
Si	1.53 × 10^{15}	RTA only	950 °C 10 s	2.9	1395	1.53	0.064	54
		PLM only	0.4 J/cm^2	31	263	13	0.29	
		PLM + RTA	950 °C 10 s	9.7	970	4.0	0.124	
Ge	8.1 × 10^{15}	RTA only	950 °C 10 s	0.81	1147	0.4	0	390
		PLM only	0.45 J/cm^2	15.6	86	7.8	0.203	
		PLM + RTA	950 °C 10 s	2.96	770	1.5	0.063	
						hole conc. p (×10^{18} cm^{-3})	E_V–E_F (eV)	
Zn	4.36 × 10^{15}	RTA only	950 °C 10 s	52.4	47	65.5	0.11	470
		PLM only	0.4 J/cm^2	270	14	338	0.33	
		PLM + RTA	950 °C 10 s	227	29	162.5	0.20	

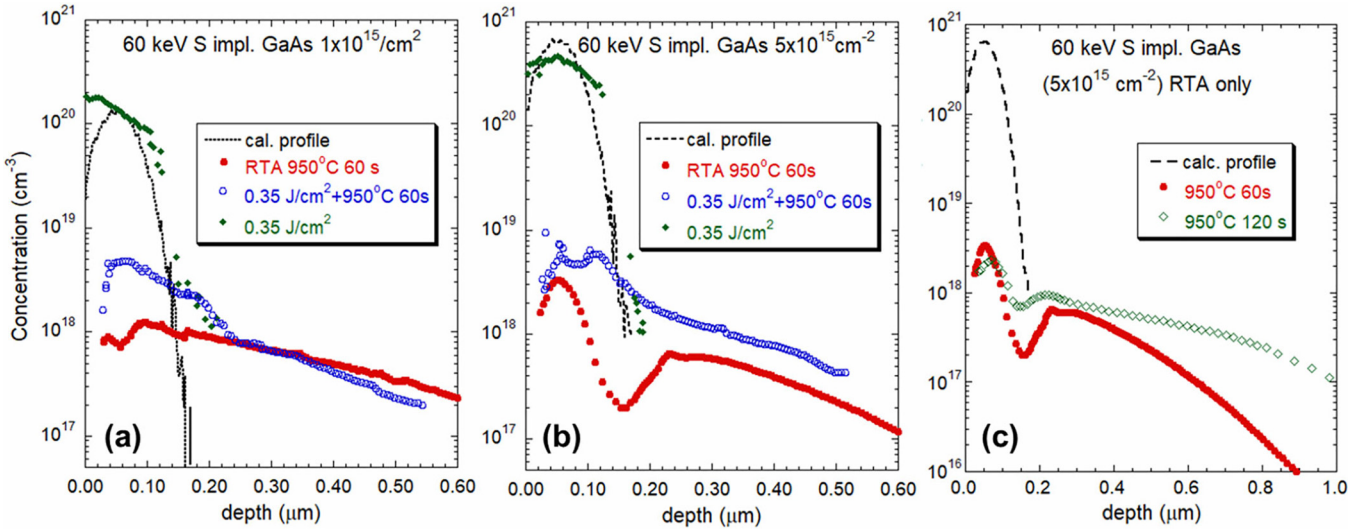

FIG. 4. ECV profiles together with the calculated S implant profiles of the (a) lo- and (b) hi-S implanted samples after RTA only, PLM only, and PLM + RTA. For both the RTA only and PLM + RTA samples, RTA was performed at 950 °C for 60 s. (c) ECV profiles of the hi-S sample after RTA only for T_{RTA} = 950 °C for 60 and 120 s.

$T_{RTA} < 600$ °C. When T_{RTA} increases further, n_s increases due to the removal of compensating defects, such as V_{Ga} and antisites. After the final RTA at 950 °C, n_s for both samples are ~2× higher, while their μ are slightly lower by ~20% compared to the corresponding RTA only samples. We note that samples RTA after PLM for a prolonged duration of 60 s at 950 °C further increases the μ and the respective n_s to 3.9×10^{13} and 4.2×10^{13} cm^{-2} for the lo- and hi-S samples. A summary of electrical properties of GaAs samples implanted with various donor species as tabulated in Table I followed by RTA only, PLM only, and PLM + RTA is shown in Table II.

Hall measurement results shown in Fig. 3 and Table II only represent the overall electrical properties of the implanted samples, but the actual electron concentration profiles can only be estimated from their assumed implantation depths. Here, we used the electrochemical capacitance–voltage (ECV) profiling method to study the depth profiles of space charges. Figure 4 shows the ECV profiles together with the calculated S implant profiles of the (a) lo- and (b) hi- S implanted samples after RTA only, PLM only, and PLM + RTA. For the PLM only samples, the net space charge concentration is close to or even exceeds the implanted S concentration. This suggests that a large fraction of these space charges is not due to the S dopant but from point defects incorporated in the top layer due to the PLM process. It is worth noting that after PLM, the space charge distribution is rather sharp and confined within ~0.14 μm. This is consistent with the estimated melt depth for the pulsed laser fluence of 0.35 J/cm^2 used for this work. For samples after RTA only and PLM + RTA, the total space charge sheet density and n_s measured by the Hall effect agree within ~20%, suggesting that the ECV profiles represent free electron distribution due to S donors. Unlike the PLM only samples, profiles from these samples also show a long diffusion tail extending to >1 μm deep. This is mainly due to the fast S diffusion in GaAs at the high T_{RTA} after PLM. Compared with the RTA only samples, the PLM + RTA samples exhibit a much higher n of $\sim 5 \times 10^{18}$ cm^{-3} as well as a flatter distribution in the implanted layer.

For the RTA only samples, the peak carrier concentrations for the lo- and hi-S samples are $\sim 1.2 \times 10^{18}$ and 3.1×10^{18} cm^{-3}, respectively. For the hi-S sample, the profile in the RTA only sample shows a notable "dip" at ~0.15 μm below the surface, which coincides with the end-of-range region of the S implantation. Such a "dip" in the net donor concentration profile is missing in the lo-S sample. This suggests that there is a significant concentration of compensating defects due to the end-of-range damage because of the high implantation dose. Figure 4(c) compares the ECV profiles of the RTA only hi-S samples at T_{RTA} = 950 °C for 60 and 120 s, showing that the dip at ~0.15 μm is significantly reduced after RTA at 950 °C for a longer duration of 120 s. Meanwhile, the S diffusion tail also extends to >1 μm after prolonged RTA. These results suggest that defects generated by the end of range implantation damage are primarily acceptor type native defects, which compensate S donors, and a $T_{RTA} > 950$ °C or annealing time >100 s is required for their removal.

Despite its amphoteric nature, Si is another common shallow donor in GaAs. In this study, we used multiple energy implantation with a total dose of 1.53×10^{15} cm^{-2} to create a relatively flat dopant distribution profile with $\sim 6.4 \times 10^{19}$ Si/cm^3 in the top ~0.24 μm in GaAs. Figure 5 shows (a) n_s and μ, and (b) ECV profiles of Si implanted GaAs samples after RTA only and PLM + RTA. Note that a slightly higher PLM fluence of 0.4 J/cm^2 was used in order to melt through the end of range damage region at ~0.3 μm below the surface. All RTA was carried out for 10 s duration. Here, the RTA only samples were highly resistive with $\rho > 10^4$ Ω cm for $T_{RTA} < 700$ °C. After RTA at 950 °C for 10 s, a n_s of 2.9×10^{13} cm^{-2} with a μ of 1390 cm^2/V s was achieved. This represents a low activation of <2% for the Si donors. Assuming a uniform distribution over ~0.24 μm, an $n \sim 1.2 \times 10^{18}$ cm^{-3} was

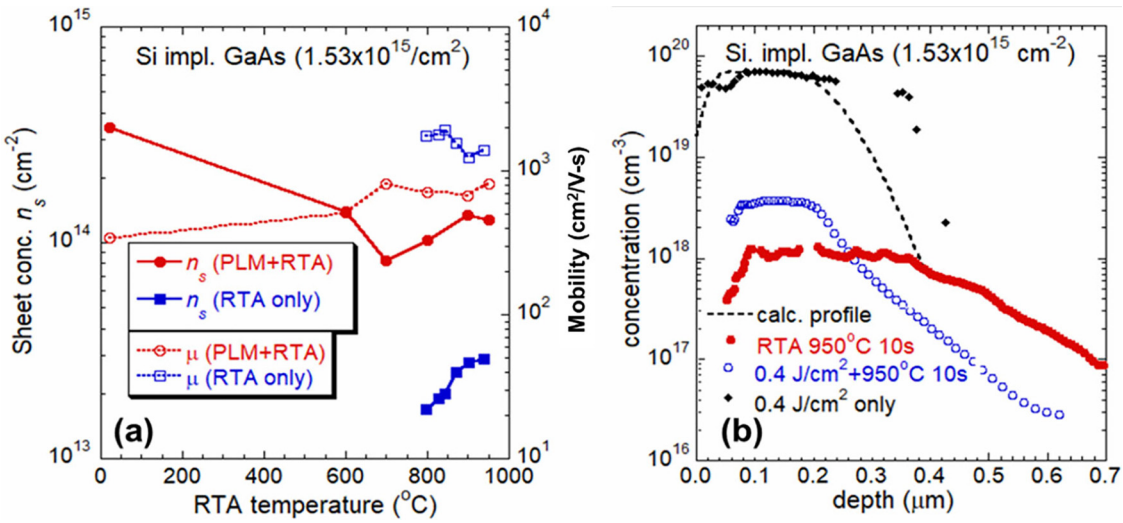

FIG. 5. (a) Hall effect measurements showing the sheet electron density n_s and mobility μ of the Si implanted GaAs samples after RTA only and PLM + RTA in the temperature range of 500–950 °C. The laser fluence for PLM was 0.4 J/cm^2, and the RTA duration was 10 s. (b) ECV profiles together with the calculated Si implant profiles after RTA only, PLM, and PLM + RTA.

estimated. This low activation is attributed, in part, to the amphoteric nature of Si and the auto-compensation by native acceptors. The Si activation was much enhanced by the rapid melt and regrowth of the PLM process. After PLM, the sample exhibits a high n_s of 3.1×10^{14} cm^{-2} or $n \sim 1.3 \times 10^{19}$ cm^{-3} but with a relatively low μ of 263 cm^2/V s. This high n corresponds to an E_F at $\sim E_{FS} + 1.1$ eV, slightly exceeding $E_{F,max}$ as predicted by the ADM. With additional RTA after PLM, similar to the S implanted case, n_s decreases, while μ increases with T_{RTA}. n for the sample after PLM + RTA at 950 °C 10 s is estimated to be $\sim 4 \times 10^{18}$ cm^{-3} with a $\mu = 970$ cm^2/V s. ECV profiles shown in Fig. 5(b) show rather uniform space charge concentration for the RTA only and PLM + RTA samples with their respective n similar to those estimated from the Hall measurements. The ECV measurement on the PLM only sample shows a high flat space charge concentration with a sharp drop, which corresponds to the melt/substrate interface. This high space charge concentration of $\sim 6 \times 10^{19}$ cm^{-3} is much higher than the n measured by the Hall effect and is related to a sum of both impurity (Si) and defect levels due to the imperfect regrowth of the implanted layer. The presence of these defects also explains the low mobility measured in the PLM sample.

Similar to Si, Ge is also a group IV amphoteric dopant in GaAs and has been shown to yield either *p*- or *n*-type GaAs when incorporated during growth or via ion implantation, depending on the growth temperature or post-implantation annealing temperature. In this study, we created a flat Ge dopant profile of $\sim 3.7 \times 10^{20}$ cm^{-3} over a thickness of $\sim 0.22\,\mu$m as shown in Fig. 1 by multiple energy implantation with a total Ge dose of 8.1×10^{15} cm^{-2}. Figure 6(a) shows the n_s and μ of samples after PLM + RTA with T_{RTA} from 650 to 950 °C. Data for samples after RTA only at 950 °C for 10 s are also shown for comparison. An n_s of 1.56×10^{14} cm^{-2} is obtained for the sample after PLM, and n_s decreases continuously and saturates at an $n_s \sim 2 \times 10^{13}$ cm^{-2} with additional RTA at >750 °C. However, a low μ of 85 cm^2/V s is observed after PLM only, which is even lower than the S and Si samples after PLM only. This low μ increases monotonically with T_{RTA} and saturates at ~770 cm^2/V s after RTA at 950 °C. The n of PLM only sample is $\sim 7.8 \times 10^{18}$ cm^{-3}, which is over an order of magnitude higher than that of the RTA only sample ($n \sim 4 \times 10^{17}$ cm^{-3}). The high n for the PLM only sample also corresponds to an E_F at ~140 meV above $E_{F,max}$. Figure 6(b) shows the ECV profiles together with the calculated Ge implant profiles after PLM and PLM + RTA. Similar to the Si implanted samples, the ECV profiles show rather uniform space charge concentration for the PLM only and PLM + RTA samples. The n of the PLM + RTA sample is similar to that estimated from the Hall measurement, but the PLM only sample shows a high flat space charge concentration, which is much higher the free electron concentration but close to the implanted dopant concentration. Again, similar to the cases of S and Si, this high space charge concentration may be related to a sum of both Ge doping and defect levels due to the imperfect regrowth of the implanted layer. Figure 6(b) also shows that the Ge diffusion is rather minor after PLM and RTA.

Compared to other donors (S and Si), both the n and μ of the Ge implanted GaAs samples are relatively low. This can be attributed to the more amphoteric nature of the dopant. As compared to Si, more of the implanted Ge are expected to incorporate in the As sublattice, which act as shallow acceptors. For example, with comparable n of ~ 1.5–2×10^{18} cm^{-3}, the μ of the RTA only lo-S and Si implanted samples are 2900 and 1395 cm^2/V s, respectively, while that of the PLM + RTA Ge implanted sample is only 770 cm^2/V s.

For all the donor species studied, n can exceed the n_{max} of $\sim 5.7 \times 10^{18}$ cm^{-3} as predicted by the ADM after PLM. However, subsequent RTA treatment after PLM results in a decrease in n to

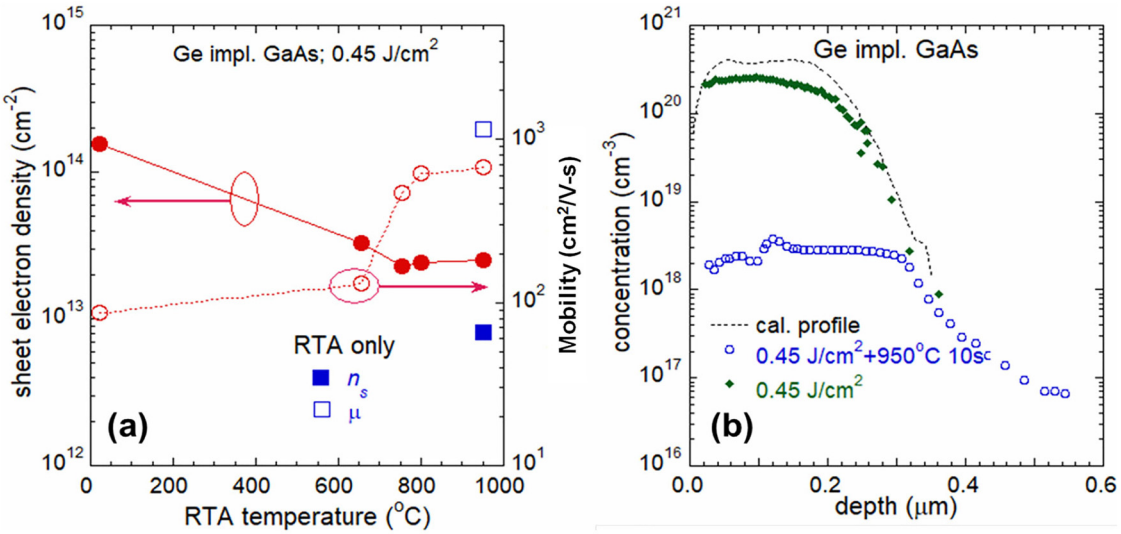

FIG. 6. (a) Hall effect measurements showing the sheet electron density n_s and mobility μ of the Ge implanted GaAs samples after PLM + RTA in the temperature range of 650–950 °C. The laser fluence for PLM was 0.45 J/cm^2, and the RTA duration was 10 s. The n_s and μ of the sample RTA only at 950 °C are also shown for comparison. (b) ECV profiles together with the calculated Ge implant profiles after PLM and PLM + RTA.

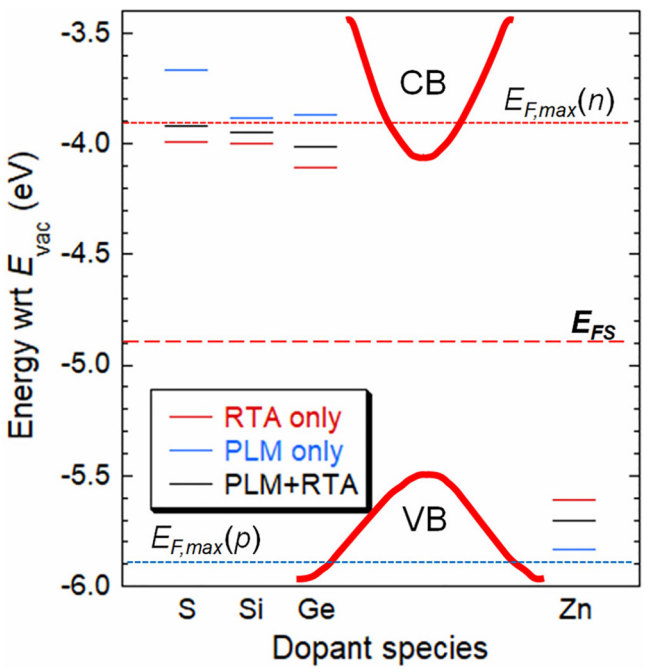

FIG. 7. Positions of the Fermi level of the GaAs samples implanted with S, Si, Ge, and Zn after RTA only, PLM only, and PLM + RTA. Positions of the E_{FS} and the $E_{F,max}$ for both *n*- and *p*-type doping as expected from the ADM are also shown with reference to the GaAs CBM and VBM.

below n_{max}, likely due to the favorable formation of compensating native acceptors. The schematic energy level diagram in Fig. 7 shows the positions of the E_F of the GaAs samples implanted with S, Si, Ge, and Zn after RTA only, PLM only, and PLM + RTA as calculated by Eq. (1). Positions of the E_{FS} and the $E_{F,max}$ for both *n*- and *p*-type doping predicted by the ADM are also shown with reference to the GaAs CBM and VBM. It is clearly seen that the non-equilibrium nature of the PLM process can achieve *n* well exceeding the equilibrium doping limit in GaAs.

In GaAs, since the position of E_{FS} is closer to the VBM, the ADM suggests that it can be doped heavily p-type to a maximum hole concentration $p_{max} > 4 \times 10^{20}$ cm^{-3} with $E_{F,max} \sim 0.4$ eV below the VBM. Here, as a comparison to the *n*-type dopants, we also studied the effect of PLM on the *p*-type doping of GaAs by Zn implantation. GaAs samples with a Zn dopant concentration of $\sim 4.4 \times 10^{20}$ cm^{-3} over a thickness of $\sim 0.08\,\mu$m were formed with multiple energy Zn ion implantation. Figure 8 shows the free hole concentration p and mobility μ of the Zn implanted GaAs samples after RTA only and PLM + RTA in the T_{RTA} range of 600–950 °C. p is estimated from the sheet hole density as measured by the Hall effect and assuming a uniform Zn distribution of 0.08 μm. Note that the as-implanted sample is already *p*-type with a low p of $\sim 5 \times 10^{18}$ cm^{-3} and μ of 1.5 cm^2/V s. Since the implantation was carried out at room temperature, the as-implanted sample is still crystalline due to the strong dynamic annealing of GaAs. This can also be observed in the c-RBS spectra of the S implanted GaAs samples shown in Fig. 2. Since the E_{FS} is closer to the VBM than the CBM in GaAs, the formation energy of native acceptor defects is lower than that of donor defects during implantation. Therefore,

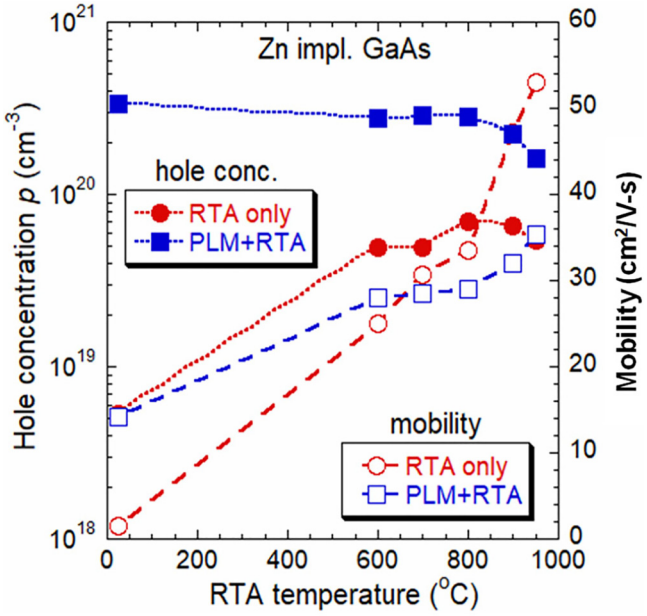

FIG. 8. Free hole concentration p and mobility μ of the Zn implanted GaAs samples after RTA only and PLM + RTA in the temperature range of 600–950 °C.

the low p observed for Zn as-implanted GaAs samples can be attributed to the net holes from Zn acceptors and native acceptor defects (e.g., V_{Ga}), while the low μ in these samples is consistent with strong scattering from crystalline defects formed during implantation. On the other hand, for n-type doping, even if some of the implanted donors are incorporated substitutionally and providing free electrons, they are compensated by the more easily formed native acceptors. This gives rise to the highly resistive nature of samples implanted with donor species. After RTA, when native defects are annealed out, and at the same time, more donors are incorporated substitutionally, the samples become n-type conducting with increasing electron concentration and mobility.

The p of the Zn implanted GaAs samples increases gradually with T_{RTA} and saturates at $\sim 6 \times 10^{19}$ cm^{-3} at 800 °C. On the other hand, μ increases to ~ 33 cm^2/V s after RTA at 800 °C and further increases more rapidly to ~ 53 cm^2/V s at 950 °C. This suggests that while the activation of Zn acceptors saturates at 800 °C, at higher T_{RTA}, crystalline defects are more effectively removed, and this enhances μ by reducing defect scattering. The μ of the RTA only samples are lower than those calculated by Walukiewicz[35] but in agreement with those reported for Zn, C, and Be doped GaAs with comparable hole concentration.[38–40] After PLM at a laser fluence of 0.4 J/cm^2, the hole concentration reaches $p \sim 3.8 \times 10^{20}$ cm^{-3}, which corresponds to an E_F of ~ 0.33 eV below the VBM. This is within the maximum $E_{F,max}$ suggested by the ADM for p-type GaAs. Similar to the cases of n-type doped GaAs, the μ of the PLM only sample is rather low at a $\mu \sim 14$ cm^2/V s. This low μ is attributed to the presence of point defects generated after the rapid melt/regrowth process. These defects can be removed by RTA after PLM as evidenced from the gradual increase in μ with RTA temperature. Note that p stays relatively stable at $\sim 3 \times 10^{20}$ cm^{-3} up to an T_{RTA} of 800 °C and drops to $\sim 1.63 \times 10^{20}$ cm^{-3} at 950 °C with a $\mu \sim 35$ cm^2/V s. The E_F positions of the Zn implanted GaAs samples calculated from the p obtained by the Hall effect measurements are also included in Fig. 7. Since the implanted Zn concentration is comparable to the expected p_{max}, the E_F for all samples shown are below the VBM but still above the $E_{F,max}$ for p-type

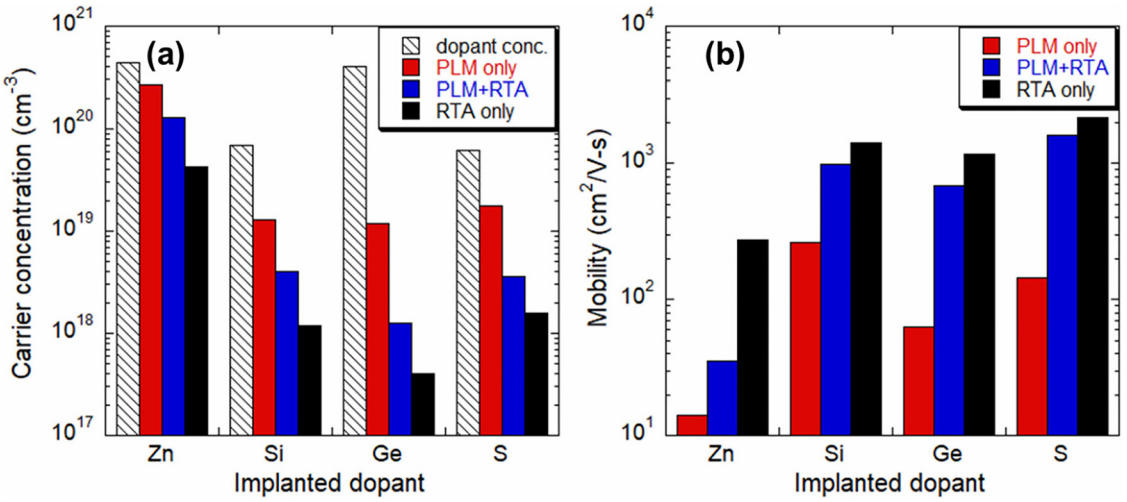

FIG. 9. A comparison of (a) the carrier concentration and (b) the mobility of GaAs implanted with various donors (S, Si, Ge) and an acceptor (Zn) after RTA only, PLM, and PLM + RTA. The approximate as-implanted dopant concentrations for the different dopants are also included in (a).

doping. Note that while E_F for the RTA only sample is >0.3 eV above the $E_{F,max}$, the E_F for PLM only sample is only <0.1 eV above $E_{F,max}$.

Figure 9 compares the electrical properties of GaAs samples implanted with donors and acceptor after RTA only, PLM only, and PLM + RTA. The calculated as-implanted dopant concentrations of all samples are plotted together with the carrier concentration (n and p) in Fig. 9(a). Note that for all dopants, n (p) after PLM is lower but close to the peak dopant concentration. This suggests that the transient PLM process is capable of trapping high concentration of dopants in the substitutional site, resulting in a carrier concentration exceeding the doping limit (for n-type) as shown in their respective E_F in Fig. 7. On the other hand, the RTA process is much less effective in trapping dopants and results in more than an order of magnitude lower carrier concentration. This lower n (p) in RTA only samples may not be the result of more compensating native acceptor defects since the mobility of these samples is not lowered. It is more likely that a higher fraction of dopants does not move into the proper substitutional site during RTA. Note that the mobility of the sample after PLM can be improved by subsequent RTA following PLM, and this is likely due to the removal of native point defects incorporated in the sample after PLM. Since most dopants are already incorporated in the substitutional site after PLM, further RTA results in a significantly higher n than the RTA only samples, although some "deactivation" of the dopants still occurs. Finally, a table comparing the n_{max} (p_{max}) in GaAs obtained in this work and by various growth and doping methods for some common dopants reported in the literature is shown in the supplementary material. Here, only some representative works with dopant concentration exceeding the maximum carrier concentration are included. n_{max} (p_{max}) achieved in this work using the PLM method significantly exceed most of the reported values in the literature. We also note that in general, a higher maximum carrier concentration (both n and p) can be obtained when the dopants were incorporated during epitaxial growth.

CONCLUSIONS

It has been known that semiconductors exhibit a "doping limitation," which is related to their conduction band minimum (CBM) and valence band maximum (VBM) positions with respect to the Fermi stabilization energy E_{FS}, which corresponds to the Fermi level at which the formation energy of donor and acceptor native defects is equal. Since the VBM is closer to E_{FS} than the CBM, the n-type doping of GaAs is limited to a free electron concentration of 10^{18}–10^{19} cm^{-3}, but it can be doped p-type to a free hole concertation of $>10^{20}$ cm^{-3}. In this work, we systematically investigated the doping limits of GaAs and compared the experimental results with predictions by the amphoteric native defect (ADM) model. Specifically, we carried out both the n- and p-type doping of GaAs via ion implantation. For n-type doping, both group VI (S) and amphoteric (Si and Ge) dopants were studied, while Zn was used as the acceptor species. In particular, implanted dopants were activated utilizing the pulsed laser melting (PLM) method in order to overcome the n-type doping limit of GaAs. We find that for all n-type dopants, while conventional rapid thermal annealing results in a similar electron concentration of $2–3 \times 10^{18}$ cm^{-3}, the transient PLM process is capable of trapping high concentration of dopants in the substitutional site and gives rise to a carrier concentration of $>10^{19}$ cm^{-3}, exceeding the doping limit of GaAs. However, the mobility of n-type GaAs after PLM is low, most likely due to scatterings from point defects generated during PLM. The low mobility of the samples after PLM can be recovered by subsequent RTA following PLM, and this is likely due to the removal of native point defects incorporated in the sample after PLM. Since most dopants are already incorporated in the substitutional site after PLM, further RTA results in a significantly higher n than the RTA only samples, although some "deactivation" of the dopants still occurs. Our results are significant to the understanding of doping mechanisms in semiconductors and provide a means for device applications that require ultra-high doping.

SUPPLEMENTARY MATERIAL

See the supplementary material for the comparison of the maximum carrier concentration in GaAs obtained in this work and by various growth and doping methods for some common dopants reported in the literature.

ACKNOWLEDGMENTS

The work performed at LBNL was supported by the Director, Office of Science, Office of Basic Energy Sciences, Materials Sciences and Engineering Division, the U.S. Department of Energy, under Contract No. DE-AC02-05CH11231. K.M.Y. acknowledges support by CityU SGP under Project No. 9380076.

AUTHOR DECLARATIONS

Conflict of Interest

The authors have no conflicts to disclose.

Author Contributions

Kin Man Yu: Conceptualization (equal); Data curation (equal); Formal analysis (equal); Funding acquisition (equal); Investigation (equal); Methodology (equal); Project administration (equal); Supervision (equal); Writing – original draft (equal); Writing – review & editing (equal). **M. A. Scarpulla:** Conceptualization (equal); Formal analysis (equal); Investigation (equal); Methodology (equal); Writing – review & editing (equal). **Chun Yuen Ho:** Investigation (equal); Methodology (equal); Writing – review & editing (equal). **O. D. Dubon:** Funding acquisition (equal); Investigation (equal); Methodology (equal); Supervision (equal); Writing – review & editing (equal). **W. Walukiewicz:** Conceptualization (equal); Data curation (equal); Investigation (equal).

DATA AVAILABILITY

The data that support the findings of this study are available from the corresponding author upon reasonable request.

REFERENCES

[1]D. B. Laks, C. G. Van de Walle, G. F. Neumark, and S. T. Pantelides, "Role of native defects in wide-band-gap semiconductors," Phys. Rev. Lett. **66**, 648–651 (1991).
[2]D. J. Chadi, "Doping in ZnSe, ZnTe, MgSe, and MgTe wide-band-gap semiconductors," Phys. Rev. Lett. **72**, 534–537 (1994).
[3]A. Garcia and J. E. Northrup, "Compensation of *p*-type doping in ZnSe: The role of impurity-native defect complexes," Phys. Rev. Lett. **74**, 1131–1134 (1995).
[4]E. Tokumitsu, "Correlation between Fermi level stabilization positions and maximum free carrier concentrations in III–V compound semiconductors," Jpn. J. Appl. Phys. **29**, L698 (1990).
[5]K. Saarinen, J. Nissilä, H. Kauppinen, M. Hakala, M. J. Puska, P. Hautojärvi, and C. Corbel, "Identification of vacancy-impurity complexes in highly n-type Si," Phys. Rev. Lett. **82**, 1883–1886 (1999).
[6]S. B. Zhang, S.-H. Wei, and A. Zunger, "Overcoming doping bottlenecks in semiconductors and wide-gap materials," Physica B **273–274**, 976–980 (1999).
[7]S. B. Zhang, "The microscopic origin of the doping limits in semiconductors and wide-gap materials and recent developments in overcoming these limits: A review," J. Phys.: Condens. Matter **14**, R881–R903 (2002).
[8]W. Walukiewicz, "Amphoteric native defects in semiconductors," Appl. Phys. Lett. **54**, 2094–2096 (1989).
[9]W. Walukiewicz, "Intrinsic limitations to the doping of wide-gap semiconductors," Physica B **302–303**, 123–134 (2001).
[10]K. M. Yu, W. Walukiewicz, W. Shan, J. W. Ager III, J. Wu, E. E. Haller, J. F. Geisz, D. J. Friedman, J. M. Olson, and S. R. Kurtz, "Nitrogen-induced enhancement of the maximum electron concentration in group III-N-V alloys," Phys. Rev. B **61**, R13337–R13340 (2000).
[11]D. T. Speaks, M. A. Mayer, K. M. Yu, S. S. Mao, E. E. Haller, and W. Walukiewicz, "Fermi level stabilization energy in cadmium oxide," J. Appl. Phys. **107**, 113706 (2010).
[12]D. M. Detert, K. B. Tom, C. Battaglia, J. D. Denlinger, S. H. N. Lim, A. Javey, A. Anders, O. D. Dubon, K. M. Yu, and W. Walukiewicz, "Fermi level stabilization and band edge energies in $Cd_xZn_{1-x}O$ alloys," J. Appl. Phys. **115**, 233708 (2014).
[13]S. B. Zhang, S.-H. Wei, and A. Zunger, "A phenomenological model for systematization and prediction of doping limits in II–VI and compounds," J. Appl. Phys. **83**, 3192–3196 (1998).
[14]J. Robertson and S. J. Clark, "Limits to doping in oxides," Phys. Rev. B **83**, 075205 (2011).
[15]X. Cai and S.-H. Wei, "Perspective on the band structure engineering and doping control of transparent conducting materials," Appl. Phys. Lett. **119**, 070502 (2021).
[16]W. Walukiewicz, "Proceedings of the 17th international conference on defects in semiconductors," Mater. Sci. Forum **143–147**, 519–530 (1993).
[17]T. Inada, S. Kato, T. Hara, and N. Toyoda, "Ohmic contacts on ion-implanted n-type GaAs layers," J. Appl. Phys. **50**, 4466–4468 (1979).
[18]S.-H. Wei, "Overcoming the doping bottleneck in semiconductors," Comput. Mater. Sci. **30**, 337–348 (2004).
[19]K. S. Jones, A. G. Lind, C. Hatem, S. Moffatt, and M. C. Ridgeway, "A brief review of doping issues in III-V semiconductors," ECS Trans. **53**, 97–105 (2013).
[20]W. Wesch and G. Götz, "Rapid annealing of ion-implanted GaAs," Phys. Status Solidi A **94**, 745–766 (1986).
[21]S. S. Gill and B. J. Sealy, "Review of rapid thermal annealing of ion implanted GaAs," J. Electrochem. Soc. **133**, 2590–2596 (1986).
[22]M. V. Rao, J. Brookshire, S. Mitra, S. B. Qadri, R. Fischer, J. Grun, N. Papanicolaou, M. Yousuf, and M. C. Ridgway, "Athermal annealing of Si-implanted GaAs and InP," J. Appl. Phys. **94**, 130–135 (2003).
[23]T. Inada, K. Tokunaga, and S. Taka, Appl. Phys. Lett. **35**, 546–548 (1979).
[24]C. W. White and P. S. Peercy, *Laser and Electron Beam Processing of Materials* (Academic Press, New York, 1980).
[25]J. S. Williams, in *Laser Annealing of Semiconductors*, edited by J. M. Poate and J. W. Mayer (Academic Press, New York, 1982), p. 385.
[26]A. Rys, Y. Shieh, D. Hal, A. Compaan, H. Yao, and A. Bhat, "Pulsed laser annealing of GaAs implanted with Se and Si," Opt. Eng. **29**, 329 (1990).
[27]C. Y. Ong, K. L. Pey, C. M. Ng, B. S. Ong, C. P. Wong, Z. X. Shen, Z. X. Xing, X. C. Wang, H. Y. Zheng, and L. Chan, "A comparative study on Si activation in GaAs between laser annealing and rapid thermal annealing," Electrochem. Solid-State Lett. **13**, H200 (2010).
[28]S. Q. Lim and J. S. Williams, "Electrical and optical doping of silicon by pulsed-laser melting," Micro **2**, 1–22 (2022).
[29]M. A. Scarpulla, K. M. Yu, O. Monteiro, M. R. Pillai, M. C. Ridgway, M. J. Aziz, and O. D. Dubon, "Ferromagnetic $Ga_{1-x}Mn_xAs$ films produced by ion implantation and pulsed laser melting," Appl. Phys. Lett. **82**, 1251–1253 (2003).
[30]K. M. Yu, W. Walukiewicz, J. W. Beeman, M. A. Scarpulla, O. D. Dubon, M. R. Pillai, and M. J. Aziz, "Enhanced nitrogen incorporation by pulsed laser annealing of GaN_xAs_{1-x} formed by N implantation," Appl. Phys. Lett. **80**, 3958–3960 (2002).
[31]K. M. Yu, W. Walukiewicz, M. A. Scarpulla, O. D. Dubon, J. Jasinski, Z. Liliental-Weber, J. Wu, J. W. Beeman, M. R. Pillai, and M. J. Aziz, "Synthesis of GaN_xAs_{1-x} thin films by pulsed laser melting and rapid thermal annealing (PLM-RTA) of N+-implanted GaAs," J. Appl. Phys. **94**, 1043–1049 (2003).
[32]S. Nojima, "Laser annealing effects in ion-implanted GaAs," J. Appl. Phys. **53**, 5028–5036 (1982).
[33]A. H. Oraby, Y. Yuba, M. Takai, K. Gamo, and S. Namba, "Pulse laser annealing effects in Si-implanted GaAs," Jpn. J. Appl. Phys. **23**, 326 (1984).
[34]P. Blood, "Capacitance-voltage profiling and the characterisation of III-V semiconductors using electrolyte barriers," Semicond. Sci. Technol. **1**, 7–27 (1986).
[35]W. Walukiewicz, "Carrier scattering by native defects in heavily doped semiconductors," Phys. Rev. B **41**, 10218–10220 (1990).
[36]D. T. J. Hurle, "Charged native point defects in GaAs and other III–V compounds," J. Cryst. Growth **237–239**, 1621–1627 (2002).
[37]E. G. Seebauer and M. C. Kratzer, "Charged point defects in semiconductors," Mater. Sci. Eng.: R: Rep. **55**, 57–149 (2006).
[38]T. Yamada, E. Tokumitsu, K. Saito, T. Akatsuka, M. Miyauchi, M. KonagaiI, and K. Takahashi, "Heavily carbon doped p-type GaAs and GaAlAs grown by metalorganic molecular bean epitaxy," J. Cryst. Growth **95**, 145–149 (1989).
[39]M. C. Hanna, Z. H. Lu, and A. Majerfeld, "Very high carbon incorporation in metalorganic vapor phase epitaxy of heavily doped p-type GaAs," Appl. Phys. Lett. **58**, 164–166 (1991).
[40]S.-I. Kim, Y. Kim, M. S. Lee, M.-S. Kim, S.-K. Min, and C. Lee, "High mobility and temperature dependent photoluminescence of carbon doped GaAs," Solid State Commun. **88**, 743–746 (1993).